Spatial Resolution Enhancement of SSM/I Data: Vegetation Studies of the Amazon Basin

David G. Long, Douglas R. Daum, and Perry J. Hardin

Electrical and Computer Engineering Dept., Brigham Young University
459 CB, Provo, UT 84602
(801) 378-4383 fax: (801) 378-6586 long@ee.byu.edu

Abstract - **The relatively low resolution of the Special Sensor Microwave/Imager (SSM/I) radiometer limits its utility in vegetation studies. However, resolution enhancement techniques can be used to ameliorate this limitation. To this end the Backus Gilbert Inversion (BGI) technique and a modified form of the the Scatterometer Image Reconstruction (SIR) algorithm are investigated as methods to create enhanced spatial resolution images from SSM/I data. A new method for generating cloud-free composite images is presented. The utility of the composite images is illustrated through a tropical vegetation discrimination study of general vegetation classes. An overall discrimination accuracy of 81.4% is achieved for 14 classes with most of the misclassification within broader vegetation categories.**

I. INTRODUCTION

While microwave radiometer data has wide application in ocean sensing, its relatively low spatial resolution limits its use in vegetation studies. Two spatial resolution enhancement algorithms have been developed for microwave data. The first, based on the Backus-Gilbert Inversion (BGI) method, has been applied to SSM/I data for both resolution enhancement and optimal interpolation [2, 7]. The second, known as the Scatterometer Image Reconstruction (SIR) algorithm [4], originally developed for Seasat-A scatterometer data, has been adapted for use with SSM/I data [3]. In this paper we compare the performance of these algorithms for generating enhanced resolution brightness images over land areas from SSM/I data. Because the images may be adversely affected by spatial variations in the atmospheric profile over the surface we have developed an algorithm to generate cloud-free enhanced resolution composite images from multiple passes of the study region. The vegetation discrimination potential of these composite SSM/I images is then explored in a simple discrimination experiment.

II. SSM/I RESOLUTION ENHANCEMENT

Ignoring the effects of the atmosphere, an SSM/I antenna temperature measurement can be modeled as the integral of the product of the surface brightness and the antenna pattern. The antenna pattern acts as a low pass filter of the surface brightness, limiting the effective resolution of the measurement. Clouds and precipitation lower the measured brightness temperature with higher frequencies progressively more sensitive. The reduction in brightness temperature can be confused with surface features. Further, the clouds attenuate the polarization differences caused by the geometric or chemical composition of different surface types. This prevents the surface polarization difference from being used to discriminate between vegetation types and/or standing water. Improving the spatial resolution and eliminating clouds can make SSM/I data more useful in vegetation studies.

A. *The Backus-Gilbert Inversion Method*

A number of authors have used Backus-Gilbert Inversion (BGI) spatial resolution and/or perform optimal interpolation of SSM/I data to either higher or lower resolution [2, 6, 7]. In resolution enhancement, BGI produces a weighted least squares estimate of the surface brightness on a rectilinear surface grid finer than the intrinsic resolution of the sensor. To estimate the brightness temperature for a given pixel, a linear combination of N "nearby" measurements is used. While there is not a unique solution for the coefficients of the linear combination, regularization permits a subjective tradeoff between noise level in the image and resolution. A noise tuning parameter, γ, which can vary from 0 to π, must be subjectively chosen and controls the tradeoff between resolution. A detailed description of the BGI algorithm is given by [6] and [7]. Following [7] the dimensional BGI tuning parameter ω is set to 0.001.

The resulting image is effected by choice of N and the relative locations and gain patterns of the nearby measurements. Restricting the size of the local region defining "nearby" measurements reduces the computational load at the expense of accuracy. Increasing N to include additional nearby measurements improves the accuracy of the resolution enhancement.

B. *The SIR Algorithm*

The Scatterometer Image Reconstruction (SIR) algorithm was originally designed to produce scatterometer images [4] but has been adapted for radiometer measurements [3]. It produces radiometric images via an iterative procedure from an initial brightness estimate. The procedure is non-linear and depends on the antenna pattern dimension, shape, and measurement overlap to obtain resolution enhancement. The SIR algorithm is a variation of the multiplicative algebraic reconstruction technique (MART), a maximum entropy reconstruction method. SIR uses a predicted value of brightness temperature of each measurement and compares that to the actual measurement to generate an update term. When measurements from multiple passes are combined, further resolution enhancement along with noise reduction is possible [4]. Multiple passes cannot be used with BGI due to the occurrence of singular matrices when two measurements fall on top of each other.

C. *Algorithm Comparison*

While BGI has previously been applied to SSM/I data [2][6][7], SIR has not been previously applied to radiometer data. Comparisons of the algorithms using simulated measurements suggest that SIR can provide higher resolution but is noisier than BGI [3]. A tradeoff between noise reduction and resolution is possible with BGI while SIR provides objective resolution enhancement.

To compare the performance of the BGI and SIR algorithms with actual data, a 19 GHz V-pol descending pass of F10 SSM/I (September, 1992) was used. The results of SIR and BGI with $\gamma = 0$ are shown in Fig. 1. Subjectively, while SIR exhibits a greater contrast along the

0-7803-3068-4/96$5.00©1996 IEEE

rivers, the BGI and SIR images appear very similar. The BGI image seems a bit smoother but not significantly more. A major difference between the algorithms is processing time. The SIR image required only 1/50 of the computation time of the BGI algorithm.

Since the results are similar for BGI and SIR, and noting the reduced computational load, we have adopted the SIR algorithm for processing the images used in this paper.

III. CLOUD REMOVAL

While multi-channel and/or multisensor algorithms for cloud removal have been developed, we use single channel enhanced resolution images to avoid introducing spurious correlation between the channels. Our algorithm is based on the idea that brightness variations over an area are caused by small-scale, temporal atmospheric effects (clouds) rather than temporal changes in the surface brightness. Using multiple passes over the surface we generate a composite image which represents the effective surface brightness temperature over a two week period. The composite image is generated from enhanced resolution images generated from each descending pass. Two weeks of similar time-of-day SSM/I data[1] (Sept. 1992) are used in the images which follow. During this period each pixel is observed from 5 to 10 times. Extending the observation period increases the number of observations but seasonal brightness variations become a greater concern.

Since the atmospheric distortion (clouds) generally lowers the brightness temperature measurements over land, high pixel values have the least atmospheric influence. Hence, [1] selected the second-highest pixel value from the measurement ensemble as the composite pixel value. To improve the performance of this algorithm, we use a modified maximum average (MMA). This algorithm estimates the cloud-free surface brightness of a pixel by choosing a subset of pixel values from the ensemble of measurements of that pixel and then averaging the selected values together. By properly selecting the subset from the ensemble, the cloud distortion is eliminated. Averaging of the subset reduces the noise and attenuates any residual bias.

In MMA the sample mean of the ensemble is computed. A subset of measurements greater than the mean is selected. The highest value of this subset is then eliminated. The average of the remaining measurements is the composite pixel value. A detailed analysis of this technique is given in [3]. The variance of the MMA estimate is lower than that of the second-highest algorithm. Like the second-highest estimate, the MMA estimate is biased high; however, the MMA bias is less than the second-highest estimate.

IV. VEGETATION DISCRIMINATION EXPERIMENT

Composite images were created for each SSM/I channel with the aid of SIR and MMA (Fig. 2). To illustrate the utility of these images, they are used in a simple tropical vegetation discrimination experiment. With the aid of a large scale vegetation map [8], large homogeneous regions are delimited for 14 different vegetation formations within a study region in central South America. Pixel values from the composite 19H, 19V, 22V, 37H, 37V, 85H and 85V images are extracted for each delimited region. Table 1 summarizes the radiometric values for the 14 vegetation formations sampled.

Generally, the brightness temperature is lower for savanna vegetation classes than for woodland and forest classes. The lack of suitable in situ data to describe the vegetation characteristics in sufficient detail, coupled with the wide range of parameter values within a given vegetation class, preclude developing detailed vegetation emission models for each vegetation class. However, a simple empirical approach can be used to initially evaluate the potential of the composite images for vegetation discrimination. Following [5] radiometric values from the composite images are used to train a simple, non-parametric, supervised classifier for the vegetation class. This approach, in effect, treats any variations of the radiometric response within a vegetation class as noise. The results provide a simple estimate of the performance which could be achieved with more sophisticated techniques or if emission-modifying effects were to be incorporated into the classifier. All 7 SSM/I channels are used in this experiment.

In the experiment one-third of the pixels from each of the vegetation formations constitute the training set for the discriminator with the remaining two-thirds acting as the withheld data set. The assignment of a pixel to a particular set is random. After training with the training set, a common first-nearest neighbor classifier is used to assign test pixels from the withheld set to a predicted vegetation class. The results of this experiment are shown in Table 2. In this table the agreement between each pixel's predicted and actual group is summarized in confusion matrix form. The quality of the supervised classification is shown as a simple percentage accuracy for each of the actual vegetation groups.

Attempts to classify the original 14 classes produced an overall classification accuracy of 81.4%. As shown in Table 2, most of the misclassification is within the broader vegetation categories. In general, the savanna and woodland categories are more accurately classified than the forest categories. The results of this simple experiment suggest that radiometer data can be used for studies of tropical vegetation.

V. CONCLUSION

A comparison of two different methods for improving the spatial resolution of SSM/I images has been presented The best-possible resolution enhancement is similar for the two algorithms. While SIR is objective and maximizes resolution enhancement, BGI permits subjective tradeoffs between resolution enhancement and noise reduction. SIR can be used with multiple passes and requires less computation. A new algorithm, the modified-maximum average (MMA) algorithm, for generating a cloud-free composite image of the surface brightness temperature has also been presented. Using these algorithms, composite images of the Amazon basin have been generated and used in a simple vegetation discrimination experiment.

[1] Courtesy of Dr. Frank Wentz of Remote Sensing Systems

REFERENCES

[1] B. Choudhury and C. Tucker, "Satellite Observed Seasonal and Inter-Annual Variation of Vegetation Over the Kalahari, The Great Victoria Desert, and The Great Sandy Desert: 1979-1984," *Remote Sensing of Environment*, Vol. 23, pp. 233-241, 1987.

[2] M.R. Farrar and E.A. Smith, "Spatial Resolution Enhancement of Terrestrial Features Using Deconvolved SSM/I Brightness Temperatures," *IEEE Trans. Geosci. Remote Sensing*, Vol. 30, no. 2, pp 349-355, March 1992.

[3] D.G. Long, D.L. Daum, and P.J. Hardin, "Vegetation Studies of the Amazon Basin Using Enhanced Resolution Seasat Scatterometer Data," submitted to the *IEEE Trans. Geosci. Remote Sensing*, 1995.

[4] D.G. Long, P.J. Hardin, and P.T. Whiting, "Resolution Enhancement of Spaceborne Scatterometer Data," *IEEE Transactions on Geoscience and Remote Sensing*, Vol. 31, No. 3, pp. 700-715, May 1993.

[5] D.G. Long and P.J. Hardin, "Vegetation Studies of the Amazon Basin Using Enhanced Resolution Seasat Scatterometer Data," *IEEE Trans. Geosci. Remote Sensing*, Vol. 32, No. 2, pp. 449-460, March 1994.

[6] G.A. Poe, "Optimum Interpolation of Imaging Microwave Radiometer Data," *IEEE Trans. Geosci. Remote Sensing*, Vol. GE-28, pp 800-810, Sept. 1990.

[7] W.D. Robinson, C. Kummerow, and W.S. Olson, "A Technique for Enhancing and Matching the Resolution of Microwave Measurements from the SSM/I Instrument," *IEEE Trans. Geosci. Remote Sensing*, Vol. 30, no. 3, pp 419-429, May 1992.

[8] UNESCO, *Vegetation Map of South America* (1:5,000,000, two sheets) and *Vegetation Map of South America Explanatory Notes*, United Nations Education, Scientific and Cultural Organization, Paris, France, 1980 and 1981.

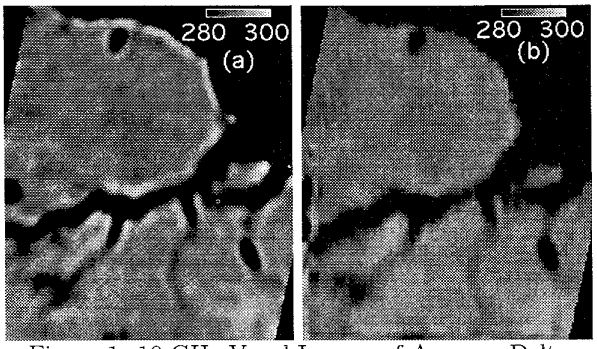

Figure 1. 19 GHz V-pol Images of Amazon Delta Region. (a) SIR. (b) BGI with $\gamma = 0$ and minimum N.

Vegetation Formation	pixels	19H (K)	19V (K)	22V (K)	37H (K)	37V (K)	85H (K)	85V (K)
Forest formations								
Extremely moist ombrophilous forest (Emf)	105	7.6	8.5	7.0	3.8	4.2	6.1	6.5
Very moist ombrophilous forest (Vmf)	2365	7.8	9.0	7.0	4.0	4.8	6.1	6.4
Moist evergreen seasonal forest (Msf)	969	8.1	9.3	8.0	4.5	5.4	7.2	7.6
Ombrophilous submontane forest (Sf)	137	4.7	7.0	5.4	1.5	2.9	4.4	5.1
Degraded forest and crops (Dfc)	48	1.3	2.2	2.8	1.8	1.0	2.6	3.8
Tropical (seasonal) evergreen lowland forest (Tse)	126	9.0	11.0	8.7	5.8	7.1	7.1	7.8
Woodland formations								
Degraded woodland and crops (Dwc)	234	10.3	12.6	9.8	6.7	8.6	8.8	9.4
Chaco (Ch)	1225	3.4	4.9	4.2	1.6	2.8	3.8	4.3
Caatinga (Ca)	414	3.8	8.0	6.9	2.8	5.7	6.1	7.2
Degraded Caatinga (Dca)	72	4.6	10.3	8.5	3.2	7.2	6.3	7.9
Savanna formations								
Campo cerrado north (Ccn)	900	6.0	12.1	9.1	4.0	8.4	6.4	8.1
Degraded campo cerrado (Dcc)	162	-1.8	3.9	2.1	-3.1	0.7	0.0	0.3
Campo cerrado south (Ccs)	408	-0.5	5.0	3.1	-1.5	2.0	0.6	1.7
Campos sujo / limpo (Csl)	472	6.0	13.0	9.3	5.5	8.5	8.7	9.1

Table 1. Mean brightness temperature for vegetation formations. Actual temperatures are obtained by adding 280 K to the tabled values.

		Actual Class												
		Forest						Woodland				Savanna			
Predicted Class		Emf	Vmf	Msf	Sf	Dfc	Tse	Dwc	Ch	Ca	Dca	Ccn	Dcc	Ccs	Csl
Forest	Emf	18	25	16	—	—	—	—	1	1	—	—	—	—	9
	Vmf	27	1280	153	12	7	23	6	48	10	—	—	—	—	16
	Msf	14	165	466	—	—	13	1	—	17	—	1	—	—	13
	Sf	2	33	—	66	1	—	—	9	7	1	—	—	—	—
	Dfc	—	1	—	—	17	—	—	—	—	—	—	—	—	—
	Tse	—	14	4	—	—	14	11	—	1	—	—	—	—	7
Woodland	Dwc	—	2	—	—	—	11	134	—	—	—	—	—	—	12
	Ch	—	48	—	2	7	—	—	741	4	—	—	—	1	—
	Ca	—	4	7	6	—	—	—	4	214	6	2	—	—	4
	Dca	—	—	—	—	—	—	—	—	12	26	4	—	—	2
Savanna	Ccn	—	—	—	—	—	1	4	—	4	13	574	—	—	21
	Dcc	—	—	—	—	—	—	—	—	—	—	—	92	16	—
	Ccs	—	—	—	—	—	—	—	—	—	—	—	13	245	—
	Csl	4	31	8	—	—	—	6	—	1	1	11	—	—	238
Total		65	1603	654	86	32	62	162	804	271	47	592	105	262	322
Percentage Correct		27.7	79.9	71.3	76.7	53.1	22.6	82.7	92.2	79.9	55.3	97.0	87.6	93.5	73.9

Table 2. Confusion matrix produced from the vegetation classification experiment. Class abbreviations are defined in Table 1.

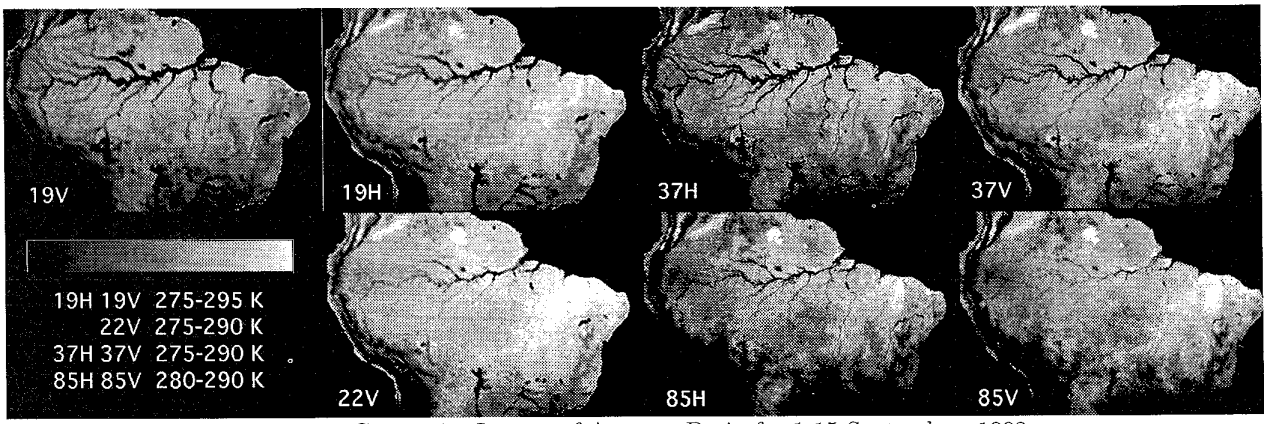

Figure 2. Composite Images of Amazon Basin for 1-15 September, 1992.